Journal of
MATERIALS RESEARCH

Characterization of nanocrystalline $\gamma-Fe_2O_3$ prepared by wet chemical method

G. Ennas,[a] G. Marongiu, and A. Musinu
Dipartimento di Scienze Chimiche, Universitá degli studi di Cagliari, Via Ospedale 72, I-09124 Cagliari, Italy

A. Falqui
Consorzio Promea, V.le R.Margherita 30, I-09124 Cagliari, Italy

P. Ballirano and R. Caminiti
Dipartimento di Chimica, Istituto Nazionale di Fisica della Materia, Universitá degli studi di Roma "La Sapienza," P.le A.Moro 5, I-00185 Roma, Italy

(Received 20 April 1998; accepted 30 September 1998)

Homogeneous maghemite ($\gamma-Fe_2O_3$) nanoparticles with an average crystal size around 5 nm were synthesized by successive hydrolysis, oxidation, and dehydration of tetrapyridino-ferrous chloride. Morphological, thermal, and structural properties were investigated by transmission electron microscopy (TEM), differential scanning calorimetry (DSC), and x-ray diffraction (XRD) techniques. Rietveld refinement indicated a cubic cell. The superstructure reflections, related to the ordering of cation lattice vacancies, were not detected in the diffraction pattern. Kinetics of the solid-state phase transition of nanocrystalline maghemite to hematite ($\alpha-Fe_2O_3$), investigated by energy dispersive x-ray diffraction (EDXRD), indicates that direct transformation from nanocrystalline maghemite to microcrystalline hematite takes place during isothermal treatment at 385 °C. This temperature is lower than that observed both for microcrystalline maghemite and for nanocrystalline maghemite supported on silica.

I. INTRODUCTION

Maghemite ($\gamma-Fe_2O_3$) is a technologically important compound widely used for the production of magnetic materials and catalysts.[1–4] Maghemite nanoparticles exhibit superparamagnetic behavior because of the small coercivity arising from a negligible energy barrier in the hysteresis of the magnetization loop.[5–9] They have recently attracted considerable interest as optical-magnetic media in magneto-optical devices. Optical-magnetic media can be made by depositing magnetic and optically transparent particles inside supporting transparent materials, and maghemite nanoparticles satisfy these requirements since they can be easily incorporated into ultrathin polymer films.[10,11]

Several preparation methods are reported in the literature aimed to prepare and to stabilize the nanometric $\gamma-Fe_2O_3$ phase.[4,7,10,12–17] Maghemite ($\gamma-Fe_2O_3$), the ferrimagnetic cubic form of iron(III) oxide, on heating transforms to hematite ($\alpha-Fe_2O_3$), the antiferromagnetic rhombohedral form. Factors like particle size, their eventual coating, and the presence of a supporting media affect the stability of iron oxides. Therefore the reported transition temperatures ($T_{\gamma\rightarrow\alpha}$) vary in the range 300–600 °C, depending also on the experimental techniques and on the heating rate adopted.[12,13,16–18]

The present study was carried out with the aim of investigating the effect of the particle size on the value of $T_{\gamma\rightarrow\alpha}$ in the absence of any support or surface coating.

Maghemite nanoparticles were prepared through the hydrolysis, oxidation, and subsequent dehydration of tetrapyridino-ferrous chloride according to a method proposed by Baudisch and Hartung.[19,20] This method avoids Fe_3O_4 (magnetite) as an intermediate phase and therefore does not require dramatic heat treatments which could favor hematite formation or grain growth.

II. EXPERIMENTAL

According to Baudisch and Hartung[19,20] the preparation was divided in two steps: (i) preparation of tetrapyridino-ferrous chloride (yellow salt) and (ii) hydrolysis and oxidation of the yellow salt to γ-ferric oxide hydrate and subsequent dehydration to maghemite.

In a typical preparation 100 mL of pure pyridine were placed in a 500 mL three neck round-bottom flask equipped with dropping funnel, CO_2 inlet tube, and bulb condenser with cold water flow in the jacket. Pyridine was freed from dissolved oxygen by heating

[a]Address all correspondence to this author.
e-mail: ennas@vaxca1.unica.it

 © 1999 Materials Research Society

it carefully to the boiling point under a vigorous flow of CO_2 through the liquid. 25 mL of saturated aqueous solution of ferrous chloride ($FeCl_2$ $4H_2O$, 98% Aldrich), prepared with fresh bidistillate and oxygen-free water in N_2 atmosphere, was dropwise added to pyridine kept in an ice bath and stirred in CO_2 atmosphere. The mixture was then allowed to stand overnight under a flow of CO_2. The obtained yellow salt was filtered in a Buchner funnel in a N_2 atmosphere, washed with small amounts of pyridine, and kept in a sealed container.

The yellow salt was then dissolved in fresh bidistillate water in the ratio of 20 g/L and placed in a flask. A vigorous oxygen flow was allowed to bubble through the solution for 15 min; a reduced flow was then continued for additional 2 h. The resulting powder, the orange γ-ferric oxide hydrate [$\gamma-$FeO(OH)], was washed in a Buchner filter with fresh bidistillate water. It was dried in argon atmosphere with a slow heating ramp and then slowly cooled to room temperature.

The final sample, dissolved in HCl, was first checked by a rapid ferricyanide test[21] to confirm the absence of Fe(II). Fe(III) content, determined by EDTA titration,[22] is consistent with Fe_2O_3 stoichiometry.

Thermal behavior of the samples was examinated by thermogravimetry (TGA) and by differential scanning calorimetry (DSC), using a Perkin-Elmer series 7 thermal analysis systems, in an argon flux and with a heating rate of 10 K/min.

TEM observations were carried out directly on the as-prepared powders without any thinning procedure using a JEOL 200CX microscope operating at 200 kV; powders were deposited on a carbon grid after being ultrasonically dispersed in octane (C. Erba, 99%).

Room temperature powder XRD data were collected on a Siemens D500 automatic powder diffractometer, operating at 35 mA and 50 kV, equipped with a graphite monochromator on the diffracted beam and using Mo K_α radiation. Warren–Averbach (W.A.) peak profile analysis[23] was performed to determine the average crystallite size. Rietveld refinement[24] was also carried out to obtain both morphological and structural information. Rietveld refinements were carried out using the PC version of the GSAS (Generalized Structure Analysis System) program.[25] A pseudo-Voigt function[26] was used to model the peak shape. The instrumental profile parameters were derived from the fitting of powder XRD data obtained from standard samples (silicon National Bureau of Standards no. 640a, microcrystalline $\gamma-Fe_2O_3$, and commercial Fe_3O_4).

Structural evolution of maghemite during isothermal treatment was observed through the *in situ* Energy Dispersive X-Ray Diffraction (EDXRD) technique using a θ-θ diffractometer equipped with a programmable furnace.[27,28] The polychromatic white beam of the tungsten bremsstrahlung was used as the source of x-rays. The diffraction data were collected in transmission mode at a fixed θ angle using a liquid nitrogen cooled Ge solid state detector.

The $\gamma-Fe_2O_3$ powder was pressed to obtain a pellet (13 mm diameter, 1 mm thickness) which was located inside the sample holder forming an angle of 5° with the incident beam. This angular value corresponds to the $0.8 \leqslant q \leqslant 4.6$ range according to the relationship $q(E, \theta) = (4\pi \sin \theta/\lambda)$. Structural evolution of the sample was followed by collecting diffraction data every 500 s after the programmed final temperature was rapidly reached.

III. RESULTS AND DISCUSSION

The precursor yellow salt and the γ-ferric oxide hydrate were characterized by XRD; peak positions and intensity correspond to $[Fe(C_6H_5N)_4]Cl_2$ and $\gamma-$FeO(OH), respectively.[29] The $\gamma-$FeO(OH) is nanocrystalline with average particle size centered around 6 nm, as approximately determined by the Scherrer method.[30]

TGA analysis of $\gamma-$FeO(OH), Fig. 1(a), indicates that the transformation to $\gamma-Fe_2O_3$ starts around 250 °C. TGA of the sample after thermal treatment for 1 h at 250 °C confirms its complete dehydration [Fig. 1(b)]. The final sample is in the form of a light-brown powder which is strongly attracted when in contact with a small natural magnet.

The bright-field TEM image of $\gamma-Fe_2O_3$ (Fig. 2) shows the presence of needle-like particles. A careful observation of the dark-field image, reported in Fig. 3, reveals, however, that each needle is formed by a chain of nanocrystals, with a narrow size distribution centered around 5 nm. Average crystal size, i.e., the average size of the coherently diffracting domains, was also evaluated by means of W.A. analysis and by Rietveld refinement.

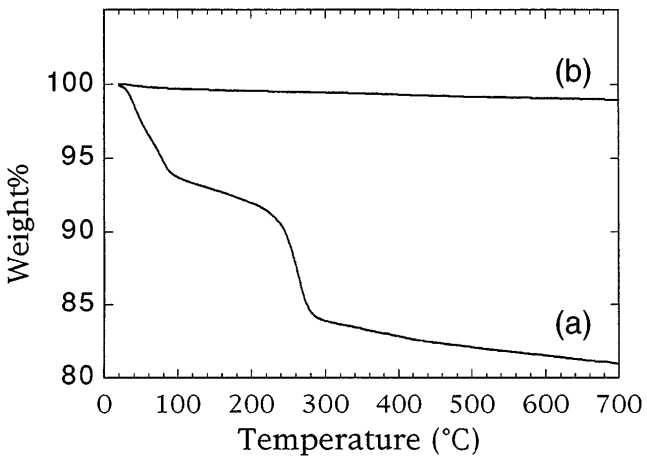

FIG. 1. Thermogravimetric curves of the (a) as-prepared γ-ferric oxide hydrate and (b) after thermal treatment at 250 °C.

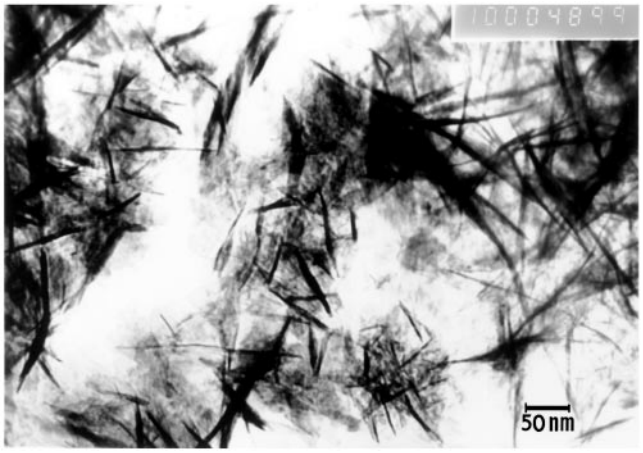

FIG. 2. Bright-field image of the nanocrystalline $\gamma-Fe_2O_3$ sample.

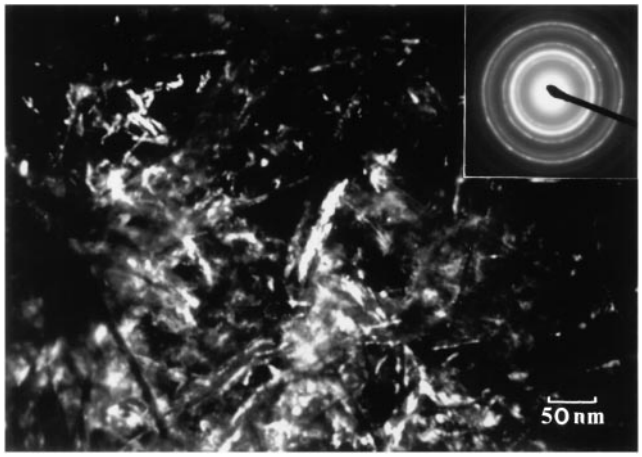

FIG. 3. Dark-field image of the nanocrystalline $\gamma-Fe_2O_3$ sample with its corresponding SAD pattern (inset).

TABLE I. Values of the average particle size $\langle D \rangle$ and relative width at half maximum (FWHM) of the size distribution curve.

	TEM	W&A	Rietveld
$\langle D \rangle$ nm	5(1)	4(1)	4(1)
FWHM nm	···	2.7(1)	···

The values are consistent with those observed in the dark-field TEM images (Table I).

Figure 4 shows the XRD pattern of the $\gamma-Fe_2O_3$ sample. Peak positions and intensity correspond to those of the reference data for $\gamma-Fe_2O_3$.[12,31–34] No trace of hematite was detected in the sample. The lattice parameter obtained by Rietveld analysis [$a = 0.8349(1)$ nm] is consistent with those obtained through selected area electron diffraction (SAED), inset of Fig. 3.

The structure of crystalline $\gamma-Fe_2O_3$ is strictly related to that of the inverse spinel Fe_3O_4. The most important difference is the presence of vacancy sites distributed on a cation sublattice. The basic

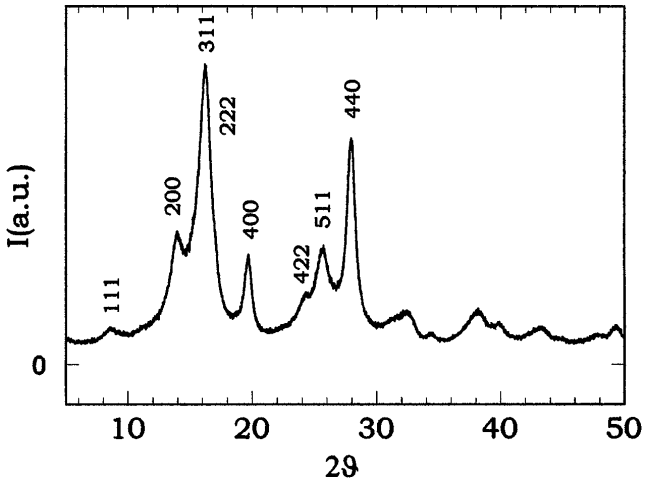

FIG. 4. Experimental x-ray powder diffraction pattern of the nanocrystalline $\gamma-Fe_2O_3$ sample.

structure of maghemite may be concisely indicated as $(Fe^{3+})_8[Fe^{3+}_{40/3}\square_{8/3}]O_{32}$ where ( ), [ ], and $\square$ designate tetrahedral, octahedral, and vacancy sites, respectively. Eight of the Fe^{3+} ions are tetrahedrally coordinated whereas the remaining are partially allocated into octahedral sites. The ordering of the vacancies gives rise to a tetragonal superstructure with $a = 0.835$ nm and $c/3 \approx 0.832$ nm.[31] The Rietveld refinement indicates a cubic cell with space group $Fd3m$. In fact, no superstructure reflections, due to the ordering of cation lattice vacancies, were observed in the diffraction pattern. This result is consistent both with a random distribution of cation vacancies among octahedral sites[31–34] and with the presence of $\gamma-Fe_2O_3$ 5 nm nanoparticles (less than 2 tetragonal cell).[13–15,18]

The values of experimental intensities of $(hh0)$ and $(h00)$ spinel reflections indicate significant preferred orientation of the $\gamma-Fe_2O_3$ nanocrystals either along crystallographic axes or parallel to the cell diagonal direction.

A broad exothermic peak centered around 390 °C, corresponding to the temperature of the γ-to-α phase transition, is present in the DSC curve of the nanocrystalline $\gamma-Fe_2O_3$ sample (Fig. 5). The XRD pattern of the powder heated up to 450 °C and then rapidly cooled down to room temperature shows all the diffraction peaks of $\alpha-Fe_2O_3$ whereas none of the $\gamma-Fe_2O_3$ was detected, indicating the completeness of phase transition.

There is a clear relation between the $T_{\gamma\to\alpha}$ and the size of maghemite nanoparticles: nanosized and ultrafine particles have $T_{\gamma\to\alpha}$ in the range 300–450 °C[6,7,12,13,16,17,35, present paper] while microcrystalline particles have $T_{\gamma\to\alpha}$ in the range 500–600 °C.[36,37] DSC data on microcrystalline maghemite particles prepared with conventional method[2] in our laboratory (inset of Fig. 5) clearly show an exothermic peak centered around

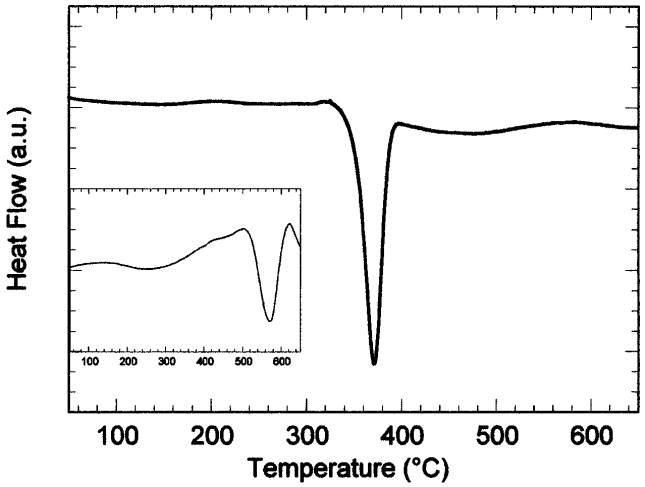

FIG. 5. DSC curves of the nanocrystalline and microcrystalline (inset) $\gamma-Fe_2O_3$ samples.

570 °C, confirming that microcrystalline $\gamma-Fe_2O_3$ is more stable in thermal treatment than nanocrystalline. The different behavior could be explained by the nonequilibrium state of nanocrystals which do not sit in an absolute minimum of free energy, but rather retain a consistent amount of excess free energy. Atoms or ions in this state need lower activation energy for diffusion,[38] and therefore thermal activated transformation occurs at lower temperatures than in equilibrium systems.[39]

We have previously shown that $T_{\gamma\rightarrow\alpha}$ of nanocrystalline maghemite supported on silica is around 700 °C.[15] From the results reported here it can be deduced that the particle-support interaction plays an important stabilization effect on the γ phase.

Kinetics of the solid state phase transition from $\gamma-$ to $\alpha-Fe_2O_3$ in the powdered sample was investigated through EDXRD. On the basis of DSC results and after a few preliminary runs, a temperature of 385 ($\pm$2) °C was chosen; at this temperature the transformation is relatively slow and can be followed in real time. Relevant time-resolved EDXRD experimental data are reported in Fig. 6: they clearly display the time course of transformation. As the reaction proceeds, the intensities of diffraction peaks of the maghemite decrease while those of hematite emerge and increase. The transition is complete after 14 h. After EDXRD measurements the thermally treated sample was analyzed by conventional XRD at room temperature (Fig. 7). All peaks belong to hematite while maghemite peaks are absent. Rietveld structural parameters are typical of microcrystalline hematite[40]; no preferred orientation effect was observed.

The evolution with time of χ, the fraction of hematite present in the sample, was calculated by the

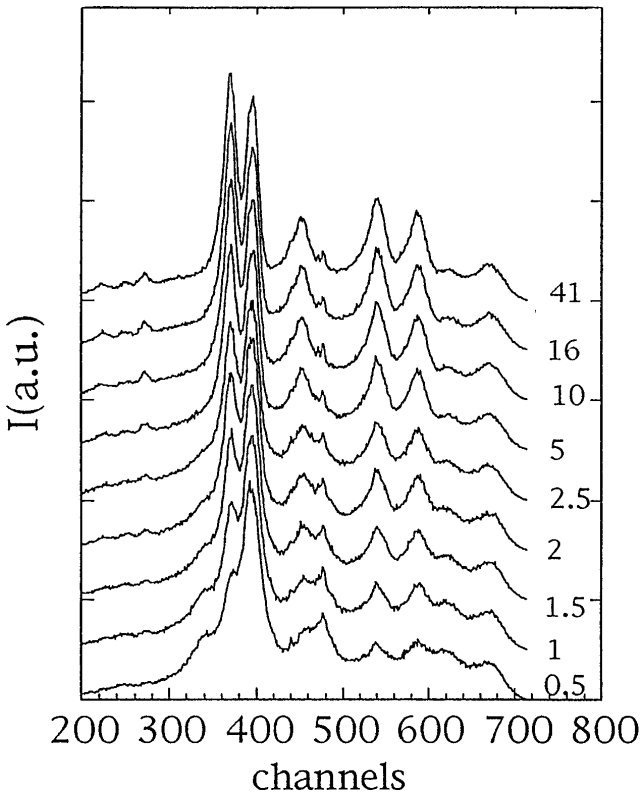

FIG. 6. Selected time-resolved, energy-dispersive x-ray diffraction spectra for the γ-to-α transformation of Fe_2O_3 at 385 °C. Acquisition time is 500 s for each spectrum; thermal treatment duration (seconds*1000) are reported.

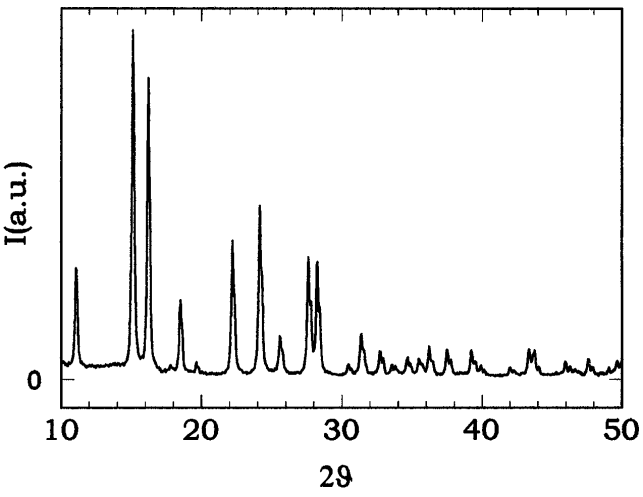

FIG. 7. Experimental x-ray powder diffraction pattern of the $\alpha-Fe_2O_3$ sample obtained after thermal treatment of the nanocrystalline $\gamma-Fe_2O_3$ sample at 385 °C in EDXRD apparatus.

following equation:

$$I(t) = \chi(t) \cdot I(t_{\text{end}}) + (1 - \chi(t)) \cdot I(t_0), \quad (1)$$

where $I(t)$, $I(t_0)$, $I(t_{\text{end}})$ are the integrated intensities. The resulting curve, reported in Fig. 8, is typical of

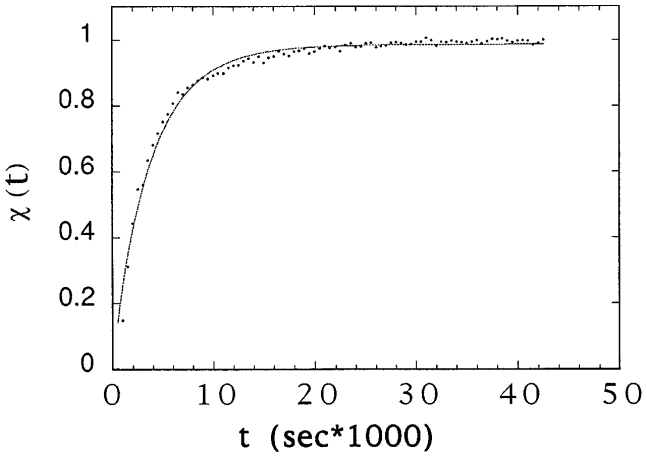

FIG. 8. Avrami equation nonlinear fit of the transformed fraction $\chi(t)$.

many solid-state transformations and is consistent with the Avrami model.[41] The nonlinear fit of the Avrami equation

$$\chi(t) = 1 - \exp(-b \cdot t^n) \qquad (2)$$

provides an n coefficient of 1.0(1). This value is typical of lineal growth of crystals when phase transition does not involve compositional change or reconstruction[39] and confirms the structural relation between $\gamma-$ and $\alpha-Fe_2O_3$ already reported in the literature for microcrystalline $\gamma-Fe_2O_3$.[36,42–44]

IV. CONCLUSIONS

The reported preparation method has proved to be suitable for the synthesis of homogeneous maghemite ($\gamma-Fe_2O_3$) nanoparticles. TEM micrographs reveal that homogeneous nanocrystals, with an average diameter around 5 nm, are connected to form needle-shaped chains 100–150 nm long. XRD analysis confirms the average crystal size obtained by TEM and gives indications for random distribution of vacancy sites in octahedral positions for $\gamma-Fe_2O_3$ cubic spinel structure. DSC results reveal that nanocrystalline $\gamma-Fe_2O_3$ is less stable than the microcrystalline one; this result is in agreement with thermodynamic considerations on the intrinsic nonequilibrium nature of nanophases.

Kinetics of the solid-state phase transformation from maghemite to hematite during isothermal treatment at 385 °C as observed by the EDXRD technique gives evidence of a displacive transition and confirms the structural relations between γ and α polymorphic forms of Fe_2O_3.

ACKNOWLEDGMENTS

The authors are particularly grateful to Professor M. Cannas for useful discussions and Mr. I. Atzeni and Mr. C. DeRubeis for technical help. This work was supported by CNR and MURST.

REFERENCES

1. M. H. Kryder, MRS Bulletin **21** (9), 17 (1996).
2. S. Onodera, H. Kondo, and T. Kawana, MRS Bulletin **21** (9), 35 (1996).
3. H. Watanabe and J. Seto, Bull. Chem. Soc. Jpn. **61**, 2411 (1991).
4. F. Hong, B. L. Yang, L. H. Schwartz, and H. H. Kung, J. Phys. Chem. **88**, 2525 (1984).
5. E. Kroll, F. M. Winnik, and R. Ziolo, Chem. Mater. **8**, 1594 (1996).
6. D. Vollath, D. V. Szabo, R. D. Taylor, J. O. Willis, and K. E. Sickafus, Nanostruct. Mater. **6**, 941 (1995).
7. F. Tronc, P. Prene, J. P. Jolivet, F. d'Orazio, F. Lucari, D. Fiorani, M. Godinho, R. Cherkaoui, M. Nogues, and J. L. Dormann, Hyperfine Interact. **95**, 129 (1995).
8. S. Linderoth, P. Hendriksen, F. Bodker, S. Wells, K. Davies, S. W. Charles, and S. Morup, J. Appl. Phys. **75**, 6583 (1994).
9. J. C. Chadwick, D. H. Jones, M. F. Thomas, C. J. Tatlock, and M. Devenish, Hyperfine Interact. **28**, 541 (1986).
10. Y. S. Kang, S. Risbud, J. F. Rabolt, and P. Stroeve, Chem. Mater. **8**, 2209 (1996).
11. R. F. Ziolo, E. P. Giannelis, B. A. Weinstein, M. P. O'Horo, B. N. Ganguly, V. Mehrotra, M. W. Russel, and D. R. Huffman, Science **257**, 219 (1992).
12. M. P. Morales, C. Pecharroman, T. Gonzáles Carreño, and C. J. Serna, J. Solid State Chem. **108**, 158 (1994).
13. P. Ayyub, M. Multani, M. Barma, and R. Viiayaraghavan, J. Phys. C **21**, 2229 (1988).
14. N. Takahashi, N. Kakuta, A. Ueno, K. Yamaguchi, T. Fujii, T. Mizushima, and Y. Udagawa, J. Mater. Sci. **26**, 497 (1991).
15. G. Ennas, A. Musinu, G. Piccaluga, D. Zedda, D. Gatteschi, C. Sangregorio, J. L. Stanger, G. Concas, and G. Spano, Chem. Mater. **10**, 495 (1998).
16. E. Tronc and J. P. Jolivet, Hyperfine Interact. **28**, 525 (1986).
17. E. Tronc, J. P. Jolivet, and J. Livage, Hyperfine Interact. **54**, 737 (1990).
18. K. Haneda and A. H. Morrish, Solid State Commun. **22**, 779 (1977).
19. O. Baudisch and W. H. Hartung, Inorg. Synth. **1**, 184 (1939).
20. O. Baudisch and W. H. Hartung, Inorg. Synth. **1**, 185 (1939).
21. F. D. Snell and L. S. Ettre, in *Encyclopedia of Industrial Chemical Analysis* (Wiley, New York, 1970–72).
22. H. A. Flaschka, in *EDTA Titrations* (Pergamon Press, London, U.K., 1959), p. 81.
23. B. E. Warren, in *X-Ray Diffraction* (Addison-Wesley, Reading, MA, 1968).
24. H. M. Rietveld, J. Appl. Crystallogr. **2**, 65 (1969).
25. R. B. Von Dreel and A. C. Larson, in *LANSCE Newsletter* no. 4, Los Alamos, NM Winter 1988.
26. C. J. Howard, J. Appl. Crystallogr. **15**, 615 (1982).
27. M. Carbone, R. Caminiti, and C. Sadun, J. Mater. Chem. **6**, 1709 (1996).
28. R. Caminiti, C. Sadun, M. Bionducci, F. Buffa, G. Ennas, G. Licheri, A. Musinu, and G. Navarra, Gazz. Chim. Ital. **127**, 59 (1997).
29. JCPDF card no. 8-98 and no. 8-524, International Center for Diffraction Data, Swarthmore, PA.
30. H. P. Klug and L. E. Alexander, in *X-Ray Diffraction Procedures for Polycrystalline Materials* (John Wiley & Sons, New York, 1974).
31. C. Greaves, J. Solid State Chem. **49**, 325 (1983).

32. A. N. Shmakov, G. N. Kryukova, V. S. Tsybhulya, A. L. Chiuviliu, and V. P. Solovyeva, J. Appl. Crystallogr. **28**, 141 (1995).
33. A. F. Wells, in *Structural Inorganic Chemistry* (Oxford Univ. Press, London, 1975).
34. C. Haas, J. Phys. Chem. Solids **26**, 1225 (1965).
35. V. Chhabra, P. Ayyub, S. Chattopadhyay, and A. N. Maitra, Mater. Lett. **26**, 21 (1996).
36. S. Kachi, K. Momiyama, and S. Shimizu, J. Phys. Soc. Jpn. **18**, 1 (1963).
37. R. M. Torrès Sánchez, J. Mater. Sci. Lett. **15**, 461 (1996).
38. S. Schumaker, R. Birringer, R. Strauss, and H. Gleiter, Acta Metall. **37**, 2485 (1989).
39. A. N. Goldsmith, C. M. Echer, and A. P. Alivisatos, Science **256**, 1425 (1992).
40. D. A. Perkins and J. P. Attfield, J. Chem. Soc. Chem. Commun. **1991**, 229 (1991).
41. M. Avrami, J. Chem. Phys. **7**, 1103 (1939) and **8**, 212 (1940).
42. S. Meillon, H. Dammak, E. Flaving, and H. Pascard, Philos. Mag. **72**, 105 (1995).
43. G. W. Oosterhout, Acta Crystallogr. **13**, 932 (1960).
44. P. Ivanov and M. Mokhov, J. Magn. Magn. Mater. **104–107**, 417 (1992).